Journal of Power Sources 219 (2012) 280–284

Contents lists available at SciVerse ScienceDirect

Journal of Power Sources

journal homepage: www.elsevier.com/locate/jpowsour

Short communication

Hollow nanotubular SnO_2 with improved lithium storage

Hong Guo [a,b,*], Rui Mao [a], Xiangjun Yang [a], Shixiong Wang [a], Jing Chen [a]

[a] School of Chemistry Science and Engineering, Yunnan University, No. 2, Green Lake North Road, Kunming 650091, Yunnan, China
[b] School of Chemistry and Chemical Engineering, Qujing Normal University, Qujing 655000, Yunnan, China

HIGHLIGHTS

- Hollow SnO_2 nanotubular materials are synthesized using kapok fibers as templates.
- The prepared nanotube is composed of nanosized SnO_2 with sizes smaller than 12 nm.
- The nanotubular electrode exhibits a stable reversible capacity of 600 mAh g^{-1}.

GRAPHICAL ABSTRACT

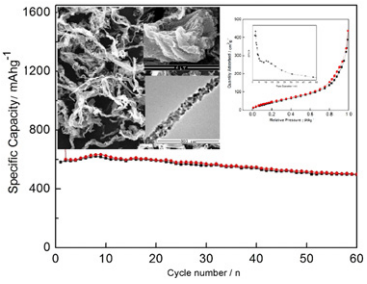

ARTICLE INFO

Article history:
Received 12 May 2012
Received in revised form
4 July 2012
Accepted 21 July 2012
Available online 2 August 2012

Keywords:
Tin oxide
Nanotube
Natural cellulose
Li-ion batteries

ABSTRACT

The approach of using cellulosic substances (kapok fibers) as templates is employed to prepare hollow SnO_2 nanotubular materials as anode materials for Li-ion batteries. The obtained nanotubular materials retain the morphological hierarchy of the kapok fibers, and each nanotube is composed of nano-sized SnO_2 ranged from 5 to 12 nm SnO_2 nanotubular anode exhibits a stable reversible capacity of 600 mAh g^{-1} at constant current density of 100 mA g^{-1}, and capacity retention keeps over 91.6% after 60 cycles. The nanostructured characteristics of SnO_2 particle embedded in the nanotube ensure the high capacity in the electrode. The nanotube came from cellulose fiber templates provides the electrode with firm framework, and thus avoids the electrode to pulverize in the charge–discharge process. Furthermore, the hollow loose structure offers a sufficient void space, which sufficiently alleviates the mechanical stress caused by volume change. All these factors contribute greatly to the excellent cycling stability of SnO_2 electrode.

1. Introduction

One of the central goals in lithium ion batteries field is to obtain high performance materials i.e. capacity, power, lifetime, and safety [1–3]. SnO_2 nanostructured materials with a high theoretically gravimetric lithium storage capacity of 782 mAh g^{-1} and the low potential of Li-ion intercalation have been considered as an attractive replacement of the graphite anodes (372 mAh g^{-1}). As anodic materials, the electrochemical processes of SnO_2 can be revealed as a two-step process. Inactive Li_2O and uniformly distributed Sn will be formed in situ during the first irreversible process, which leads to a severe capacity loss [4–6]. Then the formed metallic Sn can alloy with Li^+ in the further cycle, which is thought to be highly reversible. The formed Li_2O can act as a buffer component to improve the cycling performance of electrode and the nano-sized Sn may provide the electrode with a high specific capacity [7–9]. However, SnO_2 anode electrode suffers severe mechanical disintegration due to the drastic volumetric changes during lithium ion insertion and extraction, and therefore leads to rapid deterioration in capacity [10–12]. Large improvements have

* Corresponding author. School of Chemistry Science and Engineering, Yunnan University, No. 2, Green Lake North Road, Kunming 650091, Yunnan, China. Tel.: +86 871 5032180; fax: +86 871 5036626.
E-mail address: guohongcom@126.com (H. Guo).

0378-7753/$ – see front matter © 2012 Elsevier B.V. All rights reserved.
http://dx.doi.org/10.1016/j.jpowsour.2012.07.063

been focused on controlling the volumetric change by using nano-sized SnO_2 particles with various morphologies, such as hollow nanospheres [7–10], nanowires [12–15], nanocolloids [16], mesoporous [17] and nanobelts [18]. These materials have been proven to exhibit better electrochemical performance, suggesting that structure modification could be an effective solution to enhance the electrochemical performance [19].

In contrast to conventional methods produced nanostructured SnO_2 materials, reports on large scale synthesis of hollow nanotubular SnO_2 anodes are quite rare. SnO_2 nanotubes possess higher surfaces and a stable hollow configuration compared with conventional solid nanostructured SnO_2 materials. The former can render much contact area between Sn and Li ion in the process of electrochemical reaction, and the latter can help the active Sn to accommodate large volume change without pulverizing. Both of the factors will contribute greatly to a high specific capacity and a good cycling performance of SnO_2 nanotube anodes. However, the SnO_2 nanotubes obtained by high-temperature synthesis [20], electro-spinning of PVP/$SnCl_2{\cdot}2H_2O$ solution [21] or using cotton fibers acted as templates [22] are usually of low purity, rather nonuniform, and the hollow core is not continuous through the length of the products. Additionally, the surface areas of those materials are no more than 60 $m^2\ g^{-1}$. Herein, we propose a new strategy to prepare continuous hollow SnO_2 nanotubular materials with high purity, high surface areas and enhanced lithium storage using kapok fibers as templates in large quantities, as illustrated in Fig. 1. It is based on the surface sol–gel process as applied to covering of kapok fibers with a SnO_2 gel layer with nanometer precision. Subsequent calcinations of the as-prepared SnO_2 gel/kapok fibers composite resulted in SnO_2 nanotubes.

2. Experimental

Tin dichloride dehydrate ($SnCl_2{\cdot}2H_2O$), 2-propanol (2-C_3H_7OH), and kapok fibers were acted as raw reagents without further purification. Water used was purified using an Ulu-pure system (Shanghai, China). Surface sol–gel deposition of SnO_2 gel layers was carried out at 50 °C. The preparation procedure of SnO_2 nanotube is described as follows: 0.2 g kapok fibers was placed in a suction filter funnel, and was washed by suction filtration of ethanol, followed by drying with air flow. 0.5 g $SnCl_2{\cdot}2H_2O$ was dissolved in 20 mL 2-C_3H_7OH solution after stirring for 30 min, and then was added to the filter funnel. The solution was slowly suction-filtered through the kapok standing for 30 min to ensure adsorption of Sn^{2+} ion. Immediately 2-propanol was filtered to move the excessively adsorbed Sn^{2+} ion. Water was then added to the funnel and allowed to pass through the kapok slowly within 50 min to promote hydrolysis of $SnCl_2{\cdot}2H_2O$ and condensation of the resultant SnO_2 gel layer. Individual cellulose fibers in the kapok were thus coated with a nanometer-thick SnO_2 gel layer after dried in air. Finally, the gel heated in a furnace at 550 °C for 5 h in air to remove the original kapok template, and then white sheets composed of SnO_2 nanotubes were obtained.

X-ray diffraction (XRD) was carried out to identity the phase composition of synthesized samples over the 2θ range from 20° to 90° using a Rigaku D/max-A diffractometer with Co Kα radiation. A Fourier transform infrared spectroscope (FTIR, Themo Nicolet 670FT-IR) was used for recording the FTIR spectra of the sample ranged from 500 to 4000 cm^{-1}. Morphologies of the synthesized SnO_2 nanotubes were observed with a AMRAY 1000B scanning electron microscope (SEM), and the microstructural characteristics

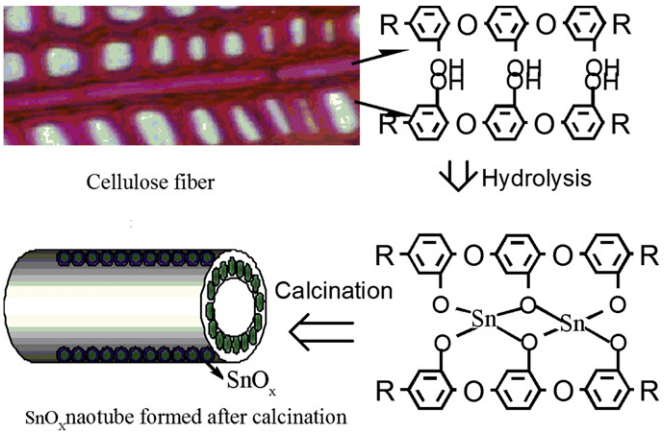

Fig. 1. Representative illustration of tin oxide nanotube synthesis by applying the surface sol–gel process on kapok fibers and subsequent calcinations in air.

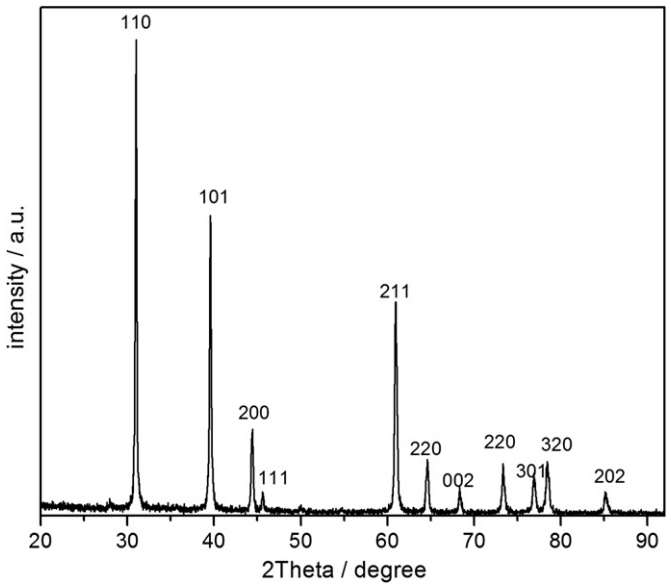

Fig. 2. XRD pattern of SnO_2 nanotubular materials synthesized by combination of the surface sol–gel process and subsequent calcinations at 550 °C.

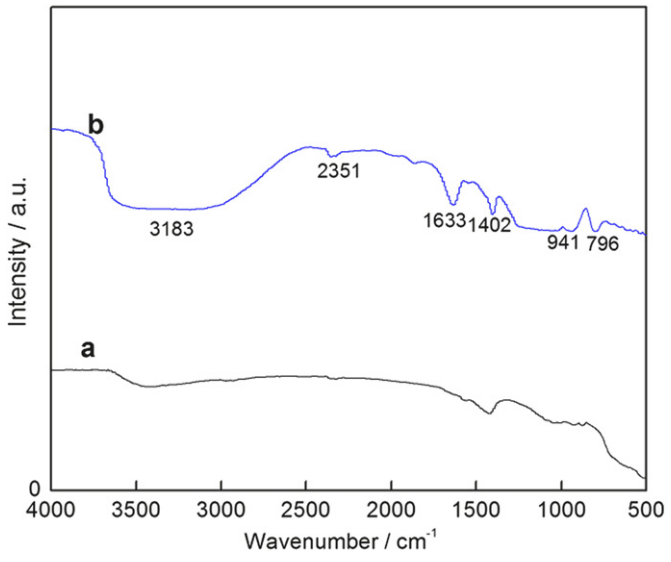

Fig. 3. FTIR spectra of the prepared SnO_2 nanotube (a) and its precursor (b).

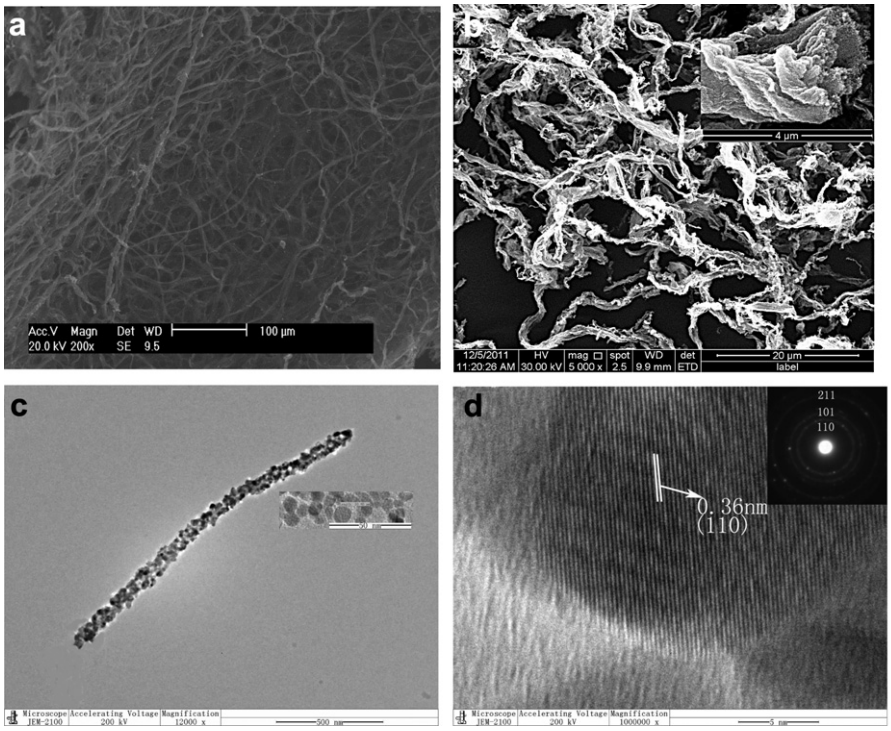

Fig. 4. SEM (a) and (b) micrograph of the kapok fibers and as-prepared SnO_2 nanotubes. TEM (c) and HRTEM (d) micrograph of SnO_2 nanotubes. The inset in (d) is the selected area electron diffraction.

of SnO_2 nanotubes were observed by high-resolution transmission electron microscope (HR-TEM, JEOL JEM-2010) working at 200 kV accelerating voltage and the lattice structure was identified by selected area electron diffraction (SAED) technique.

For electrochemical performance evaluation, half-cell studies were performed. In the experimental SnO_2 nanotubes electrode, acetylene black powder and polyvinylidene fluoride (PVDF) were used as conductive additive and binder. The synthesized SnO_2 nanotubes were mixed with acetylene black and PVDF dissolved in *N*-methyl-pyrrolidinone in the weight ratio of 85:10:5 to form slurry, which was painted on a copper foil used as current collector. After solvent evaporation, the electrode was pressed and dried at 120 °C under vacuum for 48 h. The cells were assembled in argon filled glove-box. Metallic lithium foil was used as counter electrode. The electrolyte was 1 M $LiPF_6$ in a mixture of ethylene carbonate (EC) and dimethyl carbonate (DMC) (1:1 in vol. ratio). Cycling tests were carried out at the charge and discharge current density of 100 mA g^{-1}, in the voltage range of 0.01–1.5 V versus Li/Li^+ by Land 2100A tester.

3. Results and discussion

The XRD pattern of the synthesized materials, shown in Fig. 2, declares that the product displays a tetragonal rutile SnO_2 structure (JCPDS card No. 41-1445, $a = 0.474$ nm, $c = 0.319$ nm). No other peaks are identified, indicating the samples have good phase purity.

The FTIR spectrum images of the prepared SnO_2 nanotubes and that of the precursor are shown in Fig. 3. The broad absorption peaks centered at ca. 3183, 2351 and 1633 cm^{-1} are due to adsorbed water [23]. The peak nearby 1402 cm^{-1} is corresponding to C–C bond [23]. For the precursor, the weak peaks about 941 and 796 cm^{-1} implies the presence of asymmetric stretching vibration of Sn–OH group [23]. These peaks disappeared in the spectrum of synthesized SnO_2 nanotubes, indicating these groups have decomposed after calcinations. The broad absorption peaks ranged of 500–800 cm^{-1} are assigned to Sn–O bond. The peak intensity of Sn–O bond for SnO_2 nanotubes is different from that of precursor, implying the structure of prepared sample has a little discrepancy with its precursor.

Fig. 4a and b are SEM images of the initial kapok fibers and SnO_2 nanotubes yielded by calcinations at 550 °C, respectively. The SnO_2 sheet possesses overall morphological characteristics of the initial kapok fibers except for a little shrinkage in size. The synthesized sample is SnO_2 sheet, which is composed of nanotube assemblies from the SEM morphology of cross section (the inset in Fig. 4b). The nanotubular morphology is also characterized by TEM, as illustrated in Fig. 4c, it can be clearly distinguished that the samples are

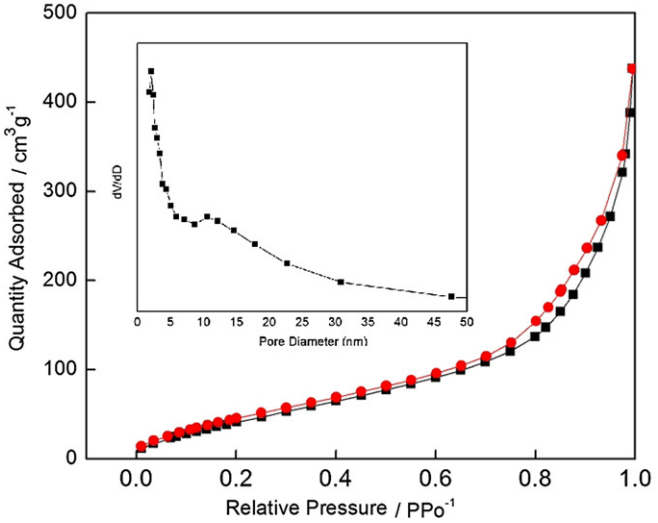

Fig. 5. Nitrogen adsorption/desorption isotherm and Barrett–Joyner–Halenda (BJH) pore size distribution plot (inset) of the prepared SnO_2 nanotubes.

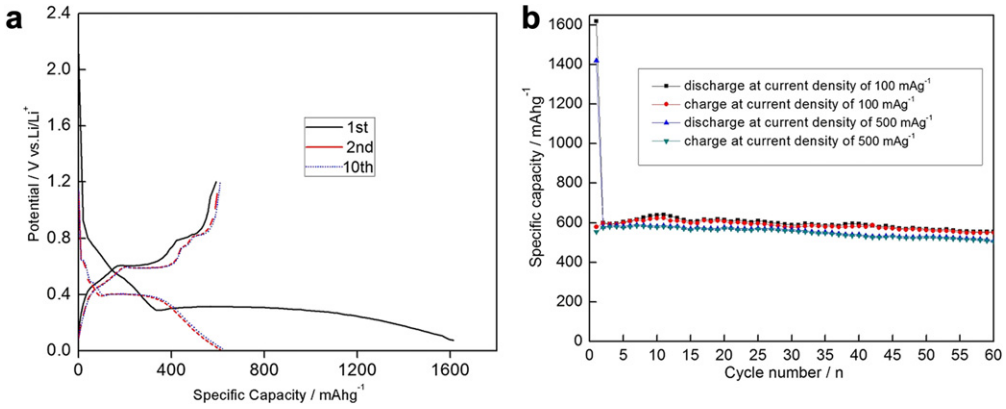

Fig. 6. Electrochemical performance of prepared SnO_2 nanotubular materials: (a) charge/discharge curves for the 1st, 2nd, and 10th cycles at current density 100 mA g^{-1}; (b) cycling performance of electrode at constant current density of 100 mA g^{-1} and 500 mA g^{-1}, respectively. Electrode potential range of 0.01–1.5 V vs. Li/Li^+.

hollow nanotubes with outer diameter ca. 50–100 nm, and the thickness of the tube wall is estimated to be 10–20 nm. Being replicas of the natural cellulose fiber, the SnO_2 nanotubes possess very high aspect ratios. The SnO_2 nanotubes are composed of fine particles with sizes smaller than 12 nm. The lattice fringe is observed obviously, and the lattice spacing (0.36 nm) agrees with rutile-phase SnO_2 (1 1 0) plane spacing from Fig. 4d. Its selected-area electron diffraction (SAED) pattern (Fig. 4d inset) reveals the diffraction rings 1–3 are indexed to (1 1 0), (1 0 1), and (2 1 1) diffraction of rutile-phase SnO_2, respectively. It indicates that the SnO_2 nanocage is composed of fine crystal particles with partial orientation. This result is in agreement with the analysis of XRD.

Fig. 5 shows the N_2 adsorption/desorption isotherms and the pore size distribution of the obtained SnO_2 nanotubes. The isotherms are identified as type IV, which is the characteristic isotherm of mesoporous materials. The pore size distribution data indicates that a majority of the pores are smaller than 25 nm. The BET surface area of the sample is 185.15 m^2 g^{-1}. The single-point total volume of pores at $P/P_0 = 0.975$ is 0.49 cm^3 g^{-1}. The BET surface area and the large total pore volume strongly indicate that the prepared SnO_2 nanotubes have a loose mesoporous structure. This structure can not only keep the nano effect of electrode but can help to buffer the volume changes of SnO_2 electrode during electrochemical reaction.

The density and conductivity of the obtained SnO_2 nanotube are 6.87 g cm^{-3} and 5.95 $\times$ 10^{-5} $\Omega^{-1}cm^{-1}$, respectively. While the conductivity of commercial SnO_2 is ca. 1.055 $\times$ 10^{-8} $\Omega^{-1}cm^{-1}$, and therefore the conductivity is enhanced a lot obviously. Lithium ions insertion into and extraction from SnO_2 are defined as discharge and charge processes in this work, respectively. The charge/discharge curves for the first two and the 10th cycles are shown in Fig. 6a. In the initial discharge, the potential drops rapidly to a plateau of 0.9 V and then decreases gradually to the plateaus of approximately 0.6 and 0.3 V. The reasons might be respectively ascribed to the formation of the solid electrolyte interface (SEI) film, Li_2O and Li_xSn ($0 \leq x \leq 4.4$) alloy, which results are consistent with other research groups [7,24,25]. From the second cycle, the initial potential plateau increases from 0.3 V to ca. 0.4 V. This voltage fluctuation may be due to the decomposition of oxides on the particle surface during the first discharge process [26]. The cycling performance profile of SnO_2 nanotubes electrode at constant current density of 100 mA g^{-1} and 500 mA g^{-1} is shown in Fig. 6b, respectively. The stable reversible capacity of electrode is 600 mAh g^{-1}, and can be retained at 550 mAh g^{-1} after 60 cycles with the retention of 91.6%. The coulombic efficiencies are always over 97.8% except for the first cycle at 100 mA g^{-1}. The initial capacity loss is 1000 mAh g^{-1}, which is relatively high. The reasons could be attributed to the formation of solid electrolyte interface (SEI) formation and the reduction of SnO_2 to Sn and Li_2O [4,27,28]. To investigate electrochemistry performance under the high rate discharge, the current density of 500 mA g^{-1} is used as constant test. The synthesized electrode also exhibits a good stability with reversible capacities of ca. 560 mAh g^{-1} and the coulombic efficiencies of 97.5–99.3%, except of the first one. Though the capacity decreases with the higher rate, the synthesized product exhibits a stable cycle capability. Compared with the previous reported SnO_2/graphene hybridization [29] and core–shell structures SnO_2 materials [7,8], the material reported here is very attractive due to its facile, economical, and improved lithium storage. Fig. 7 is the TEM image of SnO_2 nanotubular electrode materials after 60 cycles at current density 100 mA g^{-1}, which reveals that the nanotubular structure of the materials is still kept well without breakage in the process of charge–discharge. The nano-scaled characteristics of SnO_2 particle embedded in the nanotube ensure the electrode having a high capacity and a good electronic conductivity. The nanotube came from cellulose fiber template provides the electrode with a firm framework, which avoids the electrode to pulverize in the charge–discharge process. Moreover, the hollow structure offers a sufficient void space, which sufficiently alleviates

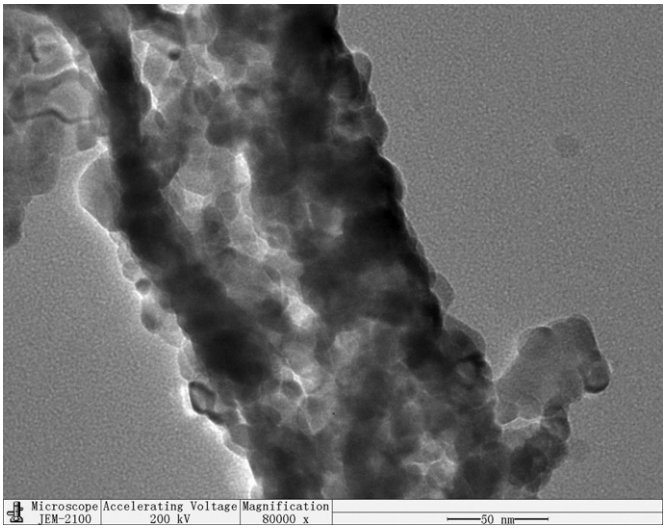

Fig. 7. TEM image of SnO_2 nanotubular electrodes after 60 cycles at current density 100 mA g^{-1}.

the mechanical stress caused by volume change. Therefore, the electrode shows an excellent cycleability.

4. Conclusions

Applied of natural cellulosic substances such as kapok fibers acted as superior templates, hollow SnO_2 nanotubular materials are synthesized by combination of the surface sol–gel process and subsequent calcination. The resulting nanotubular materials are hollow nanotubes with outer diameter ca. 50–100 nm, and the thickness of the tube wall is estimated to be 10–20 nm. Each nanotube is composed of fine particles with sizes smaller than 12 nm. Being replicas of the natural cellulose fiber, the SnO_2 nanotubes possess very high aspect ratios, and high BET surface area of 185.15 $m^2\ g^{-1}$. The stable discharge capacities of ca. 600 mAh g^{-1} and the columbic efficiencies over 97.8% were obtained at the current density of 100 mA g^{-1}. The nanostructured characteristics of SnO_2 particle embedded in the nanotube ensure the electrode having the high capacity and a good electronic conductivity. The hollow structure offers a sufficient void space, in which SnO_2 nano particles will experience a volume change without a collapse. Both of them should be responsible for the excellent cycling stability of electrode. Our strategy is simple, cheap and mass-productive, which should be suitable to large scale production of nanotubular materials used for lithium ion batteries and gas sensors.

Acknowledgments

The authors would like to acknowledge financial support provided by Department Science Foundation of China (No. 210204), Social Development Plan of Yunnan Province China (No. 2008cd148), National Natural Science Foundation of China (No. U0937601) and 863 Program of National High Technology Research Development Project of China (No. 2011AA03A405).

References

[1] J.T. Han, Y.H. Huang, B.G. John, Chem. Mater. 23 (2011) 2027–2029.
[2] A.K. Shukla1, T.P. Kumar, Curr. Sci. 94 (2008) 314–331.
[3] T.H. Mason, X.F. Liu, J. Hong, J. Graetz, E.H. Majzoub, J. Phys. Chem. C 115 (2011) 16681–16687.
[4] C. Kim, M. Noh, M. Choi, J. Cho, B. Park, Chem. Mater. 17 (2005) 3297–3301.
[5] J. Hassoun, G. Derrien, S. Panero, B. Scrosati, Adv. Mater. 20 (2008) 3169–3175.
[6] B. Cheng, J.M. Russell, W.S. Shi, L. Zhang, E.T. Samulski, J. Am. Chem. Soc. 126 (2004) 5972–5973.
[7] D. Deng, J.Y. Lee, Chem. Mater. 20 (2008) 1841–1846.
[8] X.L. Wang, M. Feygenson, M.C. Aronson, W.Q. Han, J. Phys. Chem. C 114 (2010) 14697–14703.
[9] X.W. Lou, D. Deng, J.Y. Lee, L.A. Archer, Chem. Mater. 20 (2008) 6562–6566.
[10] F. Zhang, K.X. Wang, X.Y. Wang, G.D. Li, J.S. Chen, Dalton Trans. 40 (2011) 8517–8519.
[11] C. Wang, G.H. Du, K. Ståhl, H.X. Huang, Y.J. Zhong, J.Z. Jiang, J. Phys. Chem. C 116 (2012) 4000–4011.
[12] C.M. Wang, W. Xu, J. Liu, J.G. Zhang, L.V. Saraf, B.W. Arey, Nano Lett. 11 (2011) 1874–1880.
[13] P. Meduri, C. Pendyala, V. Kumar, Nano Lett. 9 (2009) 612–616.
[14] Y.L. Wang, X.C. Jiang, Y.N. Xia, J. Am. Chem. Soc. 125 (2003) 16176–16177.
[15] H. Kim, J. Cho, J. Mater. Chem. 18 (2008) 771–775.
[16] X.W. Lou, J.S. Chen, P. Chen, L.A. Archer, Chem. Mater. 21 (2009) 2868–2874.
[17] R. D-Cakan, Y.-S. Hu, M. Antonietti, J. Maier, M.-M. Titirici, Chem. Mater. 20 (2008) 1227–1229.
[18] Z.W. Pan, Z.R. Dai, Z.L. Wang, Science 291 (2004) 1947–1949.
[19] L.W. Ji, Z. Lin, M. Alcoutlabi, X.W. Zhang, Energy Environ. Sci. 4 (2011) 2682–2699.
[20] Z.R. Dai, J.L. Gole, J.D. Stout, Z.L. Wang, J. Phys. Chem. B 106 (2002) 1274–1279.
[21] C. Gao, X. Li, B. Lu, L. Chen, Y. Wang, F. Teng, J. Wang, Z. Zhang, X. Pan, E. Xie, Nanoscale 11 (2012) 3475–3481.
[22] S. Zhu, D. Zhang, J. Gu, J. Xu, J. Dong, J. Li, J. Nanopart Res. 12 (2010) 1389–1400.
[23] P.R. Griffiths, D.J.A. Haseth, Fourier Transform Infrared Spectrometry, John Wilely & Sons, New York, 1986.
[24] R. Yang, Y. Gua, Y. Li, J. Zheng, X. Li, Acta Mater. 58 (2010) 866–874.
[25] C. Wang, Y. Zhou, M. Ge, X. Xu, Z. Zhang, J.Z. Jiang, J. Am. Chem. Soc. 132 (2010) 46–47.
[26] D. Larcher, L.Y. Beaulieu, O. Mao, A.E. George, J.R. Dahn, J. Electrochem. Soc. 147 (2000) 1703–1709.
[27] S. Han, B. Jang, T. Kim, S.M. Oh, T. Hyeon, Adv. Funct. Mater. 15 (2005) 1845–1850.
[28] X. Sun, J. Liu, Y. Li, Chem. Mater. 18 (2006) 3486–3494.
[29] S.M. Paek, E. Yoo, I.g. Honma, Nano Lett. 9 (2009) 72–75.